Fluorescence Enhancement in Topologically Optimized Gallium Phosphide All-Dielectric Nanoantennas

Cynthia Vidal, Benjamin Tilmann, Sunny Tiwari, T V Raziman, Stefan A Maier, Jérôme Wenger, Riccardo Sapienza

NANO LETTERS

pubs.acs.org/NanoLett
Letter

Fluorescence Enhancement in Topologically Optimized Gallium Phosphide All-Dielectric Nanoantennas

Cynthia Vidal,* Benjamin Tilmann, Sunny Tiwari, T. V. Raziman, Stefan A. Maier, Jérôme Wenger, and Riccardo Sapienza*

Cite This: *Nano Lett.* 2024, 24, 2437−2443

ABSTRACT: Nanoantennas capable of large fluorescence enhancement with minimal absorption are crucial for future optical technologies from single-photon sources to biosensing. Efficient dielectric nanoantennas have been designed, however, evaluating their performance at the individual emitter level is challenging due to the complexity of combining high-resolution nanofabrication, spectroscopy and nanoscale positioning of the emitter. Here, we study the fluorescence enhancement in infinity-shaped gallium phosphide (GaP) nanoantennas based on a topologically optimized design. Using fluorescence correlation spectroscopy (FCS), we probe the nanoantennas enhancement factor and observe an average of 63-fold fluorescence brightness enhancement with a maximum of 93-fold for dye molecules in nanogaps between 20 and 50 nm. The experimentally determined fluorescence enhancement of the nanoantennas is confirmed by numerical simulations of the local density of optical states (LDOS). Furthermore, we show that beyond design optimization of dielectric nanoantennas, increased performances can be achieved via tailoring of nanoantenna fabrication.

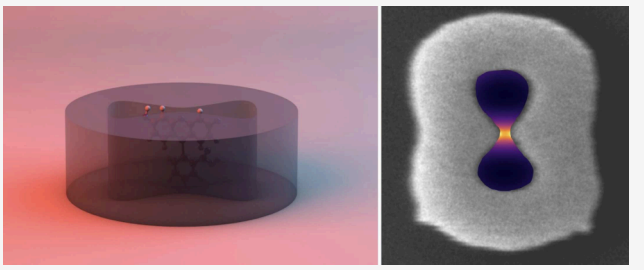

KEYWORDS: *dielectric nanoantenna, topological optimization, fluorescence correlation spectroscopy, Purcell enhancement*

Light-matter interaction can be controlled by the use of optical nanoantennas which confine light at the nanoscale, resulting in high local fields.[1] While plasmonic nanoantennas have long been used for their large Purcell enhancement factor, they suffer from strong absorption and nonradiative quenching losses. Instead, dielectric nanostructures offer moderate Purcell factor combined with close to no losses[2,3] by exploiting both electric and magnetic resonances.[4,5] Thus, dielectric nanocavities have recently been the focus of intense research in the field of nanophotonics[6,7] with applications in lasing,[8] integrated photonics,[9] nonlinear optics,[10,11] and biosensing.[12−14] In particular, gallium phosphide (GaP) presents the advantages of a high refractive index associated with close to zero absorption losses in the visible making it a material of choice to boost fluorescence emission.[10,15]

Topological optimization stands as a rapidly evolving field aiming to perfect the design of dielectric nanoantennas. The central challenge revolves around maximizing the local density of optical states (LDOS) and intensifying the light−matter interaction at the nanoscale, all achieved through the conduit of all-dielectric antennas.[16−23] This avenue not only provides a lossless alternative to plasmonic nanoantennas but also promises heightened performance. The design approaches encompass various strategies, including the utilization of evolutionary algorithms[24−26] and the optimization of electric and magnetic dipoles.[17,27,28] These efforts have coalesced into the development of generalized bowtie antennas surrounded by reflectors.

In a recent stride forward, our research group has shown that the phase distribution of point-like emitters plays a critical role, even at a deeply subwavelength scale.[29] By maximizing the in-phase backscattering into the source dipole, while concurrently mitigating the undermining impact of destructive interference, we have forged a rational architectural framework for all-dielectric antennas. Further improvement using an iterative approach has led to intense electromagnetic LDOS enhancement up to 3 orders of magnitude using a topologically optimized dielectric nanoantenna.[29]

Despite the plethora of theoretical insights into the topological optimization of dielectric nanostructures, experimental demonstrations of these hybrid nanoantennas remain sparse and predominantly confined to the near-infrared domain.[21,30,31] This preference stems from the greater ease of fabrication due to the larger wavelength and antenna dimensions. However, in the visible spectrum, the intricacies of

Received: October 2, 2023
Revised: February 7, 2024
Accepted: February 8, 2024
Published: February 14, 2024

https://doi.org/10.1021/acs.nanolett.3c03773
Nano Lett. 2024, 24, 2437−2443

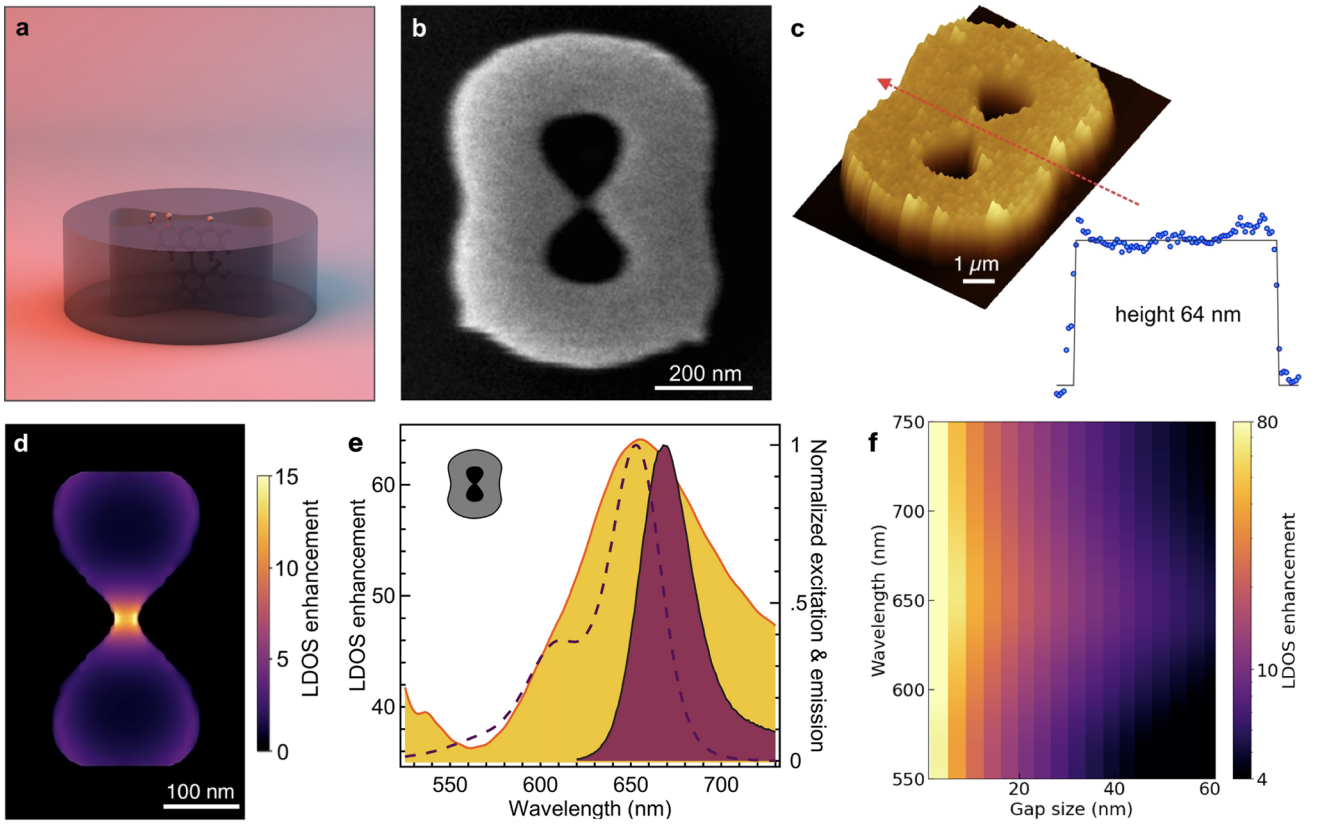

Figure 1. (a) All-dielectric topologically optimized nanoantenna to enhance the fluorescence from single diffusing molecules. (b) SEM image of a GaP nanoantenna. (c) AFM measurement of a nanoantenna. (d) Map of the LDOS enhancement at λ = 650 nm for a 30 nm gap antenna with dipole emitter aligned along the gap. (e) Overlay of the LDOS spectral enhancement (left axis, 6.5 nm gap size) and the fluorescence excitation and emission spectra of Alexa Fluor 647 used in this study (right axis). (f) 2D map of the LDOS enhancement as a function of the gap size and the emission wavelength.

nanofabrication and the imperative for precise positioning of the dipole emitter have constrained experimental endeavors.[32−34] Notably, there has yet to emerge a dielectric nanoantenna that has been both designed and characterized at optical wavelengths utilizing a topologically optimized model. This unexplored area emphasizes the importance of taking significant steps forward to connect theory with real-world applications and further advance nanophotonics.

Here, we bridge this gap and experimentally showcase the performance of gallium phosphide (GaP) nanoantennas designed according to a topologically optimized approach. Our GaP nanoantenna is shaped like the infinity symbol, with a bowtie-shaped nanogap at its center (shown in Figure 1a,b. This design, inspired by the general framework outlined in Mignuzzi's work,[29] is strategically crafted to enhance local electromagnetic effects through the precise tuning of constructive interference. Fluorescence correlation spectroscopy (FCS) experiments thoroughly characterize the GaP nanoantennas and assess their optical performance in enhancing single Alexa Fluor 647 molecule fluorescence. Our all-dielectric nanoantennas achieve a remarkable enhancement of the fluorescence brightness up to 90-fold together with optical confinement into a 200 zeptoliter (10^{-21} L) detection volume, 5000 fold below the confocal diffraction limit. These experimental values stand in excellent agreement with our numerical simulations. This successful experimental demonstration of all-dielectric topologically optimized nanoantennas in the visible spectral range holds profound significance for the realms of future sensing and quantum technologies.

The rationale behind our design departs from the quasi-static approximation to fully consider the phase of the induced polarization currents into the source dipole.[29] By enhancing the constructive interference terms and removing the negative influence of destructive interference terms, the local electromagnetic enhancement can by strategically optimized. We fabricated arrays of GaP nanoantennas using standard electron beam lithography (EBL) followed by reactive-ion etching (RIE). Details and a sketch of the nanofabrication process are illustrated in Figure S1 in Supporting Information. A scanning electron microscope (SEM) image of a typical GaP nanoantenna is shown in Figure 1b. Nanoantennas were designed with a range of gap sizes from 15 to 45 nm, with 660 nm × 510 nm dimensions. The deviations of fabricated antenna dimensions from the design, determined by SEM, are listed in SI Table S1. The GaP film thickness and roughness were determined by AFM measurements on three nanoantennas, yielding heights of H = 63.9 ± 0.53 nm and roughness of approximately 8.75 ± 0.35 nm, calculated from RMS after isolating the top structure along the line cut across the middle of the antenna (Figure 1c), and the error is the standard deviation of three measurements (Figure 1c). Due to proximity effects, the gap is often bridged below 15 ± 2.5 nm and is difficult to consistently replicate with a standard EBL setup.[35]

Numerical simulations predict an intense LDOS enhancement for the topologically optimized GaP antenna, as shown in

https://doi.org/10.1021/acs.nanolett.3c03773
Nano Lett. 2024, 24, 2437−2443

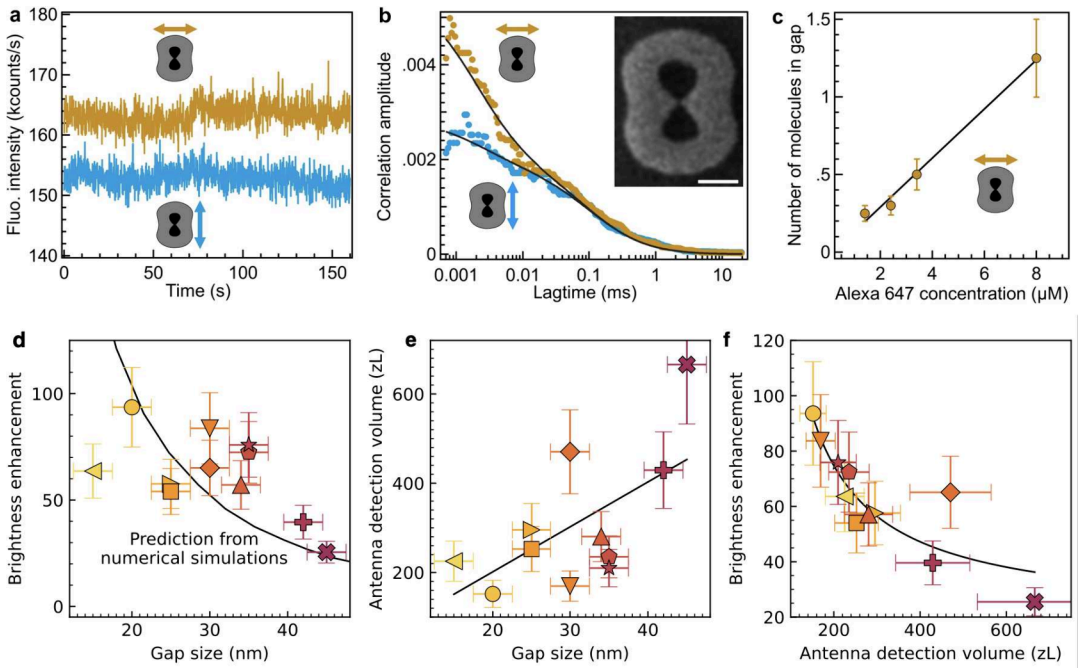

Figure 2. Experimental characterization of topologically optimized GaP nanoantennas. (a) Fluorescence intensity−time traces recorded on a 1.4 μM solution of Alexa Fluor 647 with 200 mM methylviologen on a GaP nanoantenna with the excitation polarization parallel (orange) or perpendicular (blue) to the 30 nm bowtie nanogap. The binning time is 100 ms. (b) Measured and fitted ACF g(τ) as a function of the correlation time τ from a single GaP nanoantenna with a 30 nm gap imaged in the inset. The arrows indicate the polarization direction of the laser excitation. Scale bar: 200 nm. (c) Evolution of the number of molecules in the nanogap N^* as a function of the fluorescent dye concentration. (d) Scatter plot of the fluorescence brightness enhancement as a function of the nanogap size as determined by SEM. The line is the prediction from numerical simulations, it is not a fit to the experimental data. Through (d−f), each marker symbol corresponds to a specific GaP nanoantenna. (e) Nanogap detection volume determined by FCS as a function of the nanogap size. The line fit to the data is linear. (f) Fluorescence brightness enhancement as a function of the nanogap detection volume. The line is a fit with a fixed −1 exponent. The error in brightness enhancement measurements is 20% estimated from the FCS experimental uncertainties and the data fit analysis.

Figure 1d−f. At resonance, the field is confined in the nanoantenna due to constructive interferences, leading to strong LDOS enhancement in the nanogap region between the two bowtie tips (Figure 1d). In addition, according to Maxwell's equations, the normal component of the electric displacement field remains continuous at the boundaries between two dielectrics.[16] Therefore, the size of the nanogap being much smaller than the wavelength, a strong, frequency-independent electrostatic enhancement, can be achieved for emitters aligned along the gap direction, so the LDOS enhancement effectively covers a broad spectral range (Figure 1e, f). LDOS enhancement factors exceeding 40-fold are predicted for nanogap sizes below 10 nm (Figure 1f).

We use fluorescence correlation spectroscopy (FCS) to characterize the enhancement of the fluorescence brightness for a molecule placed in the gap of the GaP nanoantenna. While placing an individual static emitter in the center of the nanogap is highly challenging,[36] FCS exploits the Brownian motion of the individual molecules diffusing in solution to probe the nanoantenna response.[37,38] FCS consists of measuring the temporal autocorrelation function (ACF) of the fluorescence signal from single molecules in order to determine their brightness. It is an established method which allows the quantification of the radiative enhancement from nanostructures.[14,39,40] The fluorescence signal is collected via a confocal microscope and detected by a single-photon counting avalanche photodetector. When the LDOS enhancement from the nanogap occurs, the shape and amplitude of the ACF are modified which in turn allow to estimate the number of molecules and their brightness enhancement within the nanogap volume.[14,40]

As a molecular probe, we use Alexa Fluor 647 dyes, with excitation wavelength at 635 nm and emission at 670 nm, where GaP is transparent (Figure 1e). 200 mM of methyl viologen is added to the buffer solution in order to quench the fluorescence quantum yield of Alexa Fluor 647 from 33% to 8% and increase the magnitude of the fluorescence enhancement factor.[41,42] This experimental configuration also enables a straightforward comparison with our earlier works using different dielectric and plasmonic antenna designs.[14,41]

Figure 2a,b displays typical experimental results on a 30 nm gap antenna probed with two different excitation polarizations parallel or perpendicular to the nanogap. We have checked that our microscope setup is polarization-insensitive so that the difference seen on the fluorescence intensity−time traces (Figure 2a) and ACFs (Figure 2b) can be directly related to the excitation of the nanogap mode which in turns leads to the fluorescence enhancement. We apply a similar analysis of the FCS fit as in our earlier studies[14,41] to extract for each antenna the average number of molecules N^* in the effective volume defined by the nanogap together with the average fluorescence brightness per emitter Q^*. From the knowledge of N^* and the fluorescent dye concentration, we can then compute the effective detection volume of the nanogap region. The fluorescence brightness enhancement is obtained by dividing the brightness per emitter in the nanogap Q^* by the reference brightness per molecule Q_0 found with the diffraction-limited confocal configuration. All the fit results for the data in Figure

https://doi.org/10.1021/acs.nanolett.3c03773
Nano Lett. 2024, 24, 2437−2443

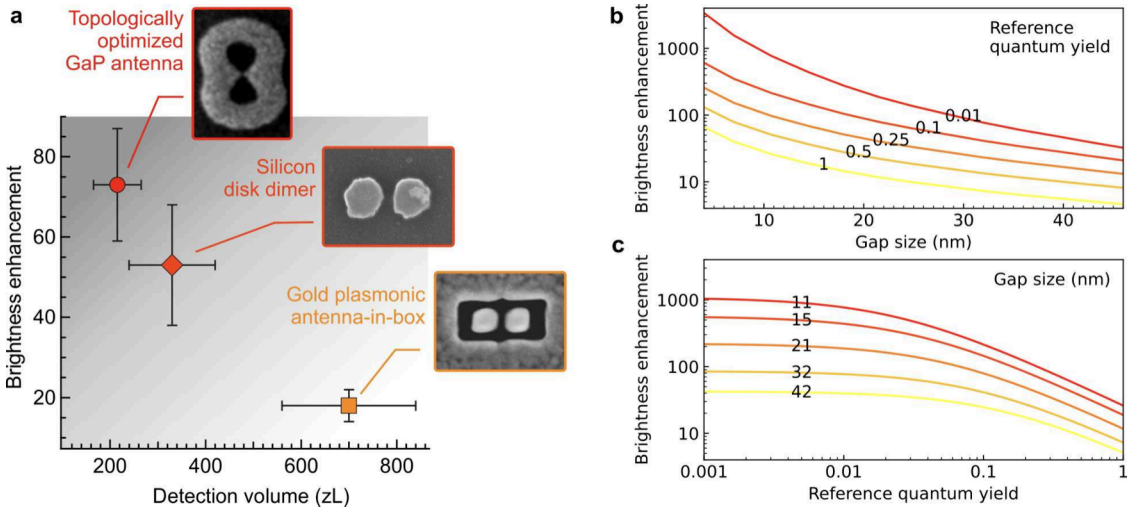

Figure 3. Comparison and performance assessment of topologically optimized GaP nanoantennas. (a) 2D map of the fluorescence enhancement and detection volume comparing different optical nanoantennas: the topologically optimized GaP antenna (this work), the silicon disk dimer[14] and the gold plasmonic antenna-in-box.[41] Importantly for the comparison, the nanoantennas indicated here all share a similar 30 nm gap and were probed using the same fluorescent dye (Alexa Fluor 647 with 200 mM methyl viologen in the buffer). (b, c) Numerical predictions of the fluorescence enhancement as a function of the nanogap size and the reference quantum yield of the emitter in homogeneous environment. In (b) the different numbers associated with each curve indicate the initial quantum yield of the emitter considered for the simulations while in (c) the numbers denote the GaP antenna gap size.

2a,b are summarized in the SI Table S2. We find a linear dependence between the number of molecules measured in the nanogap N^* and the Alexa 647 concentration used in the experiments (Figure 2c). This provides an important confirmation of the validity of our results and demonstrates a good reusability of our GaP nanoantennas.

Ideally one would like to directly record the fluorescence lifetime reduction and Purcell enhancement on each GaP nanoantenna. However, this is not currently possible in our setup for two main reasons. First, because we rely on diffusing molecules to probe the nanogap, we have to work at high micromolar concentrations and thus there is a significant number (about 500) of molecules diffusing away from the antenna hot spot but still present in the diffraction-limited confocal volume. As a result of these nonenhanced molecules contribution, there is a significant nonfluctuating fluorescence background overlaid on the antenna hot spot signal. The second reason is that to make the hot spot contribution more apparent in the FCS functions and maximize the brightness enhancement, we use low quantum yield emitters. These molecules have a short fluorescence lifetime around 380 ps[14] which is below the 600 ps resolution of our current instrument. Further accelerating the decay dynamics with the Purcell enhancement in the nanoantenna leads to a fluorescence lifetime totally beyond the capabilities of our system. This is why we rely on FCS to assess the antenna performance and cannot use Time Correlated Single Photon Counting.

For each individual nanoantenna, we correlate the gap size determined by SEM with the measured brightness enhancement (Figure 2d). Our results show a clear increase in brightness enhancement for smaller gap sizes consistent with the enhancement stemming from the hotspot in the nanogaps. Enhancement factors exceeding 60-fold are readily observed for nanogaps below 30 nm. To support our findings, we simulated the brightness enhancement using Lumerical for a dipole emitter with 8% quantum yield aligned in the center of the nanogap and an excitation intensity well below the saturation as in the experiment (see Experimental Section). The solid line in Figure 2d deduced from the numerical simulations without any free parameter shows a remarkable agreement with the experimental data.

Along with the brightness enhancement per molecule, our FCS measurements simultaneously monitor the evolution of the nanoantenna detection volume with the gap size (Figure 2e). Detection volumes below 300 zL are achieved with nanogaps below 30 nm. By integrating the Purcell factor P over the gap volume $Hdxdy$, $\frac{\int P(x,y)^* Hdxdy}{\max[P(x,y)]}$, in the numerical simulations in Figure 1d, we can estimate a detection volume around 400 zL which comes close to the 215 ± 50 zL measured for 30 nm gap antennas with FCS. The nanogap volume scales linearly with the gap size (Figure 2e) while the LDOS enhancement in the gap decays inversely proportional to the gap size as seen from simulations (Figure 2d). Since the brightness enhancement is proportional to the square of LDOS enhancement for low-quantum yield emitters, we expect the brightness enhancement to decay slightly sublinearly with the mode volume when accounting for the background enhancement contribution from the antenna. This observed correlation echoes findings from previous studies on gold dimer nanoantennas,[40] reaffirming the credibility of our results.

The nanoantenna with a 15 nm gap does not follow this trend. This may be the consequence of fabrication imperfections such as reduced hotspot efficiency due to a nonsmooth nanogap, or high losses due to an increase in the imaginary part of the refractive index.[21] Alternatively, individual molecules might be unable to access the center of the smaller nanogap due to reduced Brownian motion and/or blockage from nonfluorescent buffer molecules adsorbed onto the GaP. However, as the only antenna with such a small gap, we must be careful about generalizing the deteriorated performance.

The optical performance of these topologically optimized GaP nanoantennas significantly outperforms the values

https://doi.org/10.1021/acs.nanolett.3c03773
Nano Lett. 2024, 24, 2437−2443

achieved using silicon nanodisk dimers[14] or gold antenna-in-box[41] with similar gap sizes. To ensure a fair comparison, we focus on nanoantennas with similar 30 nm gap sizes probed under similar experimental conditions with the same fluorescent dye. Figure 3a shows a bidimensional map allowing to compare at a glance between the brightness enhancement and the detection volume achieved with different nanogap antennas. Importantly, our topologically optimized nanoantenna outperforms its competitors on both the brightness enhancement and the optical confinement, demonstrating the superiority of its rational phase optimization design.[29]

The excellent agreement found between the experimental data and the numerical simulations in Figure 2d allows us to elaborate on the simulations to predict the conditions leading to maximum brightness enhancement. The results summarized in Figure 3b, c predict enhancement factors exceeding 1000-fold for all-dielectric GaP nanoantennas, albeit for emitters with quantum yields below 2% and gap sizes below 10 nm. This positive insight holds promising implications for the realm of all-dielectric nanophotonics, providing an added incentive to enhance nanofabrication technology and attain sub-10 nm gaps. A narrowing of the nanogap is clearly one of the best ways to improve a nanoantenna's performance, however it remains extremely challenging to consistently control on multiple structures.[43−45]

In conclusion, we have successfully demonstrated the superior optical performance of all-dielectric GaP nanoantennas designed according to a topologically optimized approach. Thanks to a precise tuning of interferences occurring in the near field of the emitter,[29] the LDOS enhancement is maximized, leading to intense brightness enhancement of single quantum emitters. Nanoantennas capable of large fluorescence enhancement with minimal absorption losses are key elements to advance optical technologies from single-photon sources to biosensing. Therefore, this experimental demonstration of all-dielectric topologically optimized nanoantennas in the visible spectral range holds profound significance for the realms of future sensing and quantum technologies. Beyond the design optimization using a rational approach, increased antenna performances can be achieved via tailoring the nanofabrication to reach smaller gaps. Localizing the emitter into the nanogap, controlling its orientation or using new high refractive index materials like transition metal dichalcogenides are other future optimization directions.

EXPERIMENTAL SECTION

Nanofabrication. Here, we base the nanoantenna design on the one from ref 29, i.e., 50 nm thick, 550 nm long, and 10 nm gap size. For this, a GaP film is deposited on a glass substrate using sputter deposition at 350 °C. Next, the nanofabrication is carried out using EBL and subsequent RIE, as sketched in Figure S1 in the Supporting Information. Poly(methyl methacrylate) (PMMA) is used as photoresist and the EBL process is carried out at an acceleration voltage of 30 kV and an aperture size of 30 μm. Afterward, the development is done by rinsing the sample in a mixture of methyl isobutyl ketone and isopropyl alcohol (ratio 1:3) for 45 s. The gold mask is then deposited using electron-beam evaporation at ultrahigh vacuum, with a dedicated thickness of 40 nm. After the lift-off in an acetone bath, where the remaining PMMA is dissolved, the designed structures remain as gold mask on top of the GaP film. Finally, the structures are transferred into the GaP by performing inductively coupled plasma RIE based on chlorine gases, after which the remaining gold is removed by respective wet chemistry.

Optical Microscopy Experiments. The FCS measurements are performed using a custom-built confocal microscope (Nikon Ti−U Eclipse) equipped with a water immersion objective (Zeiss C-Apochromat 63x, 1.2 NA). A focused linearly polarized pulsed laser at 635 nm, with 70 ps pulse duration and 40 MHz repetition rate (LDH series laser diode, PicoQuant) illuminates individual nanoantennas. The antenna sample is immersed in a buffer solution of Alexa Fluor 647 at micromolar concentration with 200 mM methyl viologen as a quencher and 10 mM glutathione as an antioxidant and photostabilizer. Methyl viologen is used to improve the antenna apparent brightness enhancement and make the FCS signature from the nanogap stand out more clearly. With this 200 mM methyl viologen concentration, the quantum yield of the Alexa Fluor 647 dyes is quenched down to 8%.[14,41] The fluorescence emission in the 650 to 690 nm range is collected by the same microscope objective in the epifluorescence mode. A multiband dichroic mirror (ZT 405/488/561/640rpc, Chroma) and emission filters (ZET405/488/565/640mv2 and ET655 from Chroma plus one FF01−676/37 from Semrock) reject the baskscattered laser light. Detection is performed with a single-photon counting avalanche photodiode (PerkinElmer SPCM AQR 13) whose output is connected to a time-correlated single photon counting module (HydraHarp 400, Picoquant). Throughout all our experiments, the laser power measured at the microscope back entrance is kept constant at 2 μW and the total integration time per FCS experiment is 240 s. To efficiently remove the afterpulsing artifacts in the ACFs, we implement the FLCS correction following the approach in ref 46 and the built-in function in Symphotime64 (Picoquant).

Fluorescence Correlation Spectroscopy Analysis. FCS computes the temporal correlation of the fluorescence signal $\langle I(t)\cdot I(t+\tau)\rangle/\langle I(t)\rangle^2$, where τ is the delay (lag) time, and $\langle\ \rangle$ indicates time averaging. Our analysis approach builds on the similar methodology used for our earlier studies on plasmonic[39−41] and dielectric nanoantennas.[14] The total fluorescence signal is considered to be composed to two parts: the enhanced fluorescence from molecules within the nanogap and the fluorescence from the molecules away from the nanogap yet still present within diffraction-limited confocal volume. An essential feature in FCS is that the molecules contribute to G in proportion to the square of their fluorescence brightness, so that the fluorescence from molecules in the nanogap region experiencing the maximum enhancement will have a major contribution in the FCS correlation. See SI for details on the fit analysis.

Numerical Simulations. We performed electrodynamic simulations using Lumerical, a commercial finite difference time domain (FDTD) solver.[47] For details on the numerical simulations, see SI.

ASSOCIATED CONTENT

Supporting Information

The Supporting Information is available free of charge at https://pubs.acs.org/doi/10.1021/acs.nanolett.3c03773.

Additional information on nanofabrication, FCS fit, and numerical simulations (PDF)

https://doi.org/10.1021/acs.nanolett.3c03773
Nano Lett. 2024, 24, 2437−2443

AUTHOR INFORMATION

Corresponding Authors

Cynthia Vidal − *Blackett Laboratory, Department of Physics, Imperial College London, London SW7 2AZ, U.K.;* orcid.org/0000-0001-6183-4269; Email: c.vidal@imperial.ac.uk

Riccardo Sapienza − *Blackett Laboratory, Department of Physics, Imperial College London, London SW7 2AZ, U.K.;* orcid.org/0000-0002-4208-0374; Email: r.sapienza@imperial.ac.uk

Authors

Benjamin Tilmann − *Nano-Institute Munich, Department of Physics, Ludwig-Maximilians-University Munich, 80539 Munich, Germany;* orcid.org/0000-0002-8998-6667

Sunny Tiwari − *Aix Marseille Univ, CNRS, Centrale Marseille, Institut Fresnel, 13013 Marseille, France*

T. V. Raziman − *Department of Mathematics, Imperial College London, London SW7 2AZ, U.K.; Blackett Laboratory, Department of Physics, Imperial College London, London SW7 2AZ, U.K.;* orcid.org/0000-0002-7085-6934

Stefan A. Maier − *School of Physics and Astronomy, Monash University, Clayton, Victoria 3800, Australia; Blackett Laboratory, Department of Physics, Imperial College London, London SW7 2AZ, U.K.;* orcid.org/0000-0001-9704-7902

Jérôme Wenger − *Aix Marseille Univ, CNRS, Centrale Marseille, Institut Fresnel, 13013 Marseille, France;* orcid.org/0000-0002-2145-5341

Complete contact information is available at: https://pubs.acs.org/10.1021/acs.nanolett.3c03773

Notes

The authors declare no competing financial interest.

ACKNOWLEDGMENTS

This work has received funding from the European Union's Horizon 2020 research and innovation programme under the Marie Skłodowska-Curie grant agreement No. 882135-Bright-Nano-vdW and the European Research Council (ERC) grant agreement 723241. This work was funded by EXC 2089/1-390776260. The authors also acknowledge the support of EPSRC (EP/T027258/1 and EP/P033431/1). S.A.M. additionally acknowledges the LeeLucas Chair in Physics and the Centre of Excellence in Future Low-Energy Electronics Technologies, Australian Research Council (CE170100039).

REFERENCES

(1) Novotny, L.; Hecht, B. *Principles of Nano-Optics*; Cambridge University Press, 2006.

(2) Krasnok, A. E.; Miroshnichenko, A. E.; Belov, P. A.; Kivshar, Y. S. All-dielectric optical nanoantennas. *Opt. Express, OE* **2012**, *20*, 20599−20604.

(3) Kuznetsov, A. I.; Miroshnichenko, A. E.; Brongersma, M. L.; Kivshar, Y. S.; Luk'yanchuk, B. Optically resonant dielectric nanostructures. *Science* **2016**, *354*, aag2472.

(4) Staude, I.; Miroshnichenko, A. E.; Decker, M.; Fofang, N. T.; Liu, S.; Gonzales, E.; Dominguez, J.; Luk, T. S.; Neshev, D. N.; Brener, I.; Kivshar, Y. Tailoring Directional Scattering through Magnetic and Electric Resonances in Subwavelength Silicon Nanodisks. *ACS Nano* **2013**, *7*, 7824−7832.

(5) Yang, Y.; Zenin, V. A.; Bozhevolnyi, S. I. Anapole-Assisted Strong Field Enhancement in Individual All-Dielectric Nanostructures. *ACS Photonics* **2018**, *5*, 1960−1966.

(6) Yan, J.; Liu, X.; Ma, C.; Huang, Y.; Yang, G. All-dielectric materials and related nanophotonic applications. *Materials Science and Engineering: R: Reports* **2020**, *141*, 100563.

(7) Koshelev, K.; Favraud, G.; Bogdanov, A.; Kivshar, Y.; Fratalocchi, A. Nonradiating photonics with resonant dielectric nanostructures. *Nanophotonics* **2019**, *8*, 725−745.

(8) Koshelev, K.; Kivshar, Y. Dielectric Resonant Metaphotonics. *ACS Photonics* **2021**, *8*, 102−112.

(9) Díaz-Escobar, E.; Barreda, A. I.; Mercadé, L.; Griol, A.; Pitanti, A.; Martínez, A. Light Guidance Aided by the Toroidal Dipole and the Magnetic Quadrupole in Silicon Slotted-Disk Chains. *ACS Photonics* **2023**, *10*, 707−714.

(10) Cambiasso, J.; Grinblat, G.; Li, Y.; Rakovich, A.; Cortés, E.; Maier, S. A. Bridging the Gap between Dielectric Nanophotonics and the Visible Regime with Effectively Lossless Gallium Phosphide Antennas. *Nano Lett.* **2017**, *17*, 1219−1225.

(11) Frizyuk, K.; Melik-Gaykazyan, E.; Choi, J.-H.; Petrov, M. I.; Park, H.-G.; Kivshar, Y. Nonlinear Circular Dichroism in Mie-Resonant Nanoparticle Dimers. *Nano Lett.* **2021**, *21*, 4381−4387.

(12) Ghenuche, P.; Mivelle, M.; de Torres, J.; Moparthi, S. B.; Rigneault, H.; Van Hulst, N. F.; García-Parajó, M. F.; Wenger, J. Matching Nanoantenna Field Confinement to FRET Distances Enhances Förster Energy Transfer Rates. *Nano Lett.* **2015**, *15*, 6193−6201.

(13) Cambiasso, J.; König, M.; Cortés, E.; Schlücker, S.; Maier, S. A. Surface-Enhanced Spectroscopies of a Molecular Monolayer in an All-Dielectric Nanoantenna. *ACS Photonics* **2018**, *5*, 1546−1557.

(14) Regmi, R.; Berthelot, J.; Winkler, P. M.; Mivelle, M.; Proust, J.; Bedu, F.; Ozerov, I.; Begou, T.; Lumeau, J.; Rigneault, H.; García-Parajó, M. F.; Bidault, S.; Wenger, J.; Bonod, N. All-Dielectric Silicon Nanogap Antennas To Enhance the Fluorescence of Single Molecules. *Nano Lett.* **2016**, *16*, 5143−5151.

(15) Sortino, L.; Zotev, P. G.; Phillips, C. L.; Brash, A. J.; Cambiasso, J.; Marensi, E.; Fox, A. M.; Maier, S. A.; Sapienza, R.; Tartakovskii, A. I. Bright single photon emitters with enhanced quantum efficiency in a two-dimensional semiconductor coupled with dielectric nano-antennas. *Nat. Commun.* **2021**, *12*, 6063.

(16) Robinson, J. T.; Manolatou, C.; Chen, L.; Lipson, M. Ultrasmall Mode Volumes in Dielectric Optical Microcavities. *Phys. Rev. Lett.* **2005**, *95*, 143901.

(17) Liang, X.; Johnson, S. G. Formulation for scalable optimization of microcavities via the frequency-averaged local density of states. *Opt. Express* **2013**, *21*, 30812−30841.

(18) Wang, F.; Christiansen, R. E.; Yu, Y.; Mørk, J.; Sigmund, O. Maximizing the quality factor to mode volume ratio for ultra-small photonic crystal cavities. *Appl. Phys. Lett.* **2018**, *113*, 241101.

(19) Molesky, S.; Lin, Z.; Piggott, A. Y.; Jin, W.; Vucković, J.; Rodriguez, A. W. Inverse design in nanophotonics. *Nature Photon* **2018**, *12*, 659−670.

(20) Wu, T.; Gurioli, M.; Lalanne, P. Nanoscale Light Confinement: the Qs and Vs. *ACS Photonics* **2021**, *8*, 1522−1538.

(21) Albrechtsen, M.; Vosoughi Lahijani, B.; Christiansen, R. E.; Nguyen, V. T. H.; Casses, L. N.; Hansen, S. E.; Stenger, N.; Sigmund, O.; Jansen, H.; Mørk, J.; Stobbe, S. Nanometer-scale photon confinement in topology-optimized dielectric cavities. *Nat. Commun.* **2022**, *13*, 6281.

(22) Albrechtsen, M.; Vosoughi Lahijani, B.; Stobbe, S. Two regimes of confinement in photonic nanocavities: bulk confinement versus lightning rods. *Opt. Express* **2022**, *30*, 15458−15469.

(23) Yang, Y.; Wang, Y.; Yan, Y.; Cheng, W.; Zhao, Q.; Li, Y. On-Chip Single-Molecule Fluorescence Enhancement via Slotted Gallium Phosphide Nanodisks at Anapole States. Advanced. *Opt. Mater.* **2024**, *12*, 2301444.

(24) Gondarenko, A.; Preble, S.; Robinson, J.; Chen, L.; Lipson, H.; Lipson, M. Spontaneous Emergence of Periodic Patterns in a

Biologically Inspired Simulation of Photonic Structures. *Phys. Rev. Lett.* **2006**, *96*, 143904.
(25) Gondarenko, A.; Lipson, M. Low modal volume dipole-like dielectric slab resonator. *Opt. Express* **2008**, *16*, 17689−17694.
(26) Bonod, N.; Bidault, S.; Burr, G. W.; Mivelle, M. Evolutionary Optimization of All-Dielectric Magnetic Nanoantennas. Advanced. *Opt. Mater.* **2019**, *7*, 1900121.
(27) Hu, S.; Weiss, S. M. Design of Photonic Crystal Cavities for Extreme Light Concentration. *ACS Photonics* **2016**, *3*, 1647−1653.
(28) Brûlé, Y.; Wiecha, P.; Cuche, A.; Paillard, V.; Colas des Francs, G. Magnetic and electric Purcell factor control through geometry optimization of high index dielectric nanostructures. *Opt. Express* **2022**, *30*, 20360.
(29) Mignuzzi, S.; Vezzoli, S.; Horsley, S. A. R.; Barnes, W. L.; Maier, S. A.; Sapienza, R. Nanoscale Design of the Local Density of Optical States. *Nano Lett.* **2019**, *19*, 1613−1617.
(30) Hu, S.; Khater, M.; Salas-Montiel, R.; Kratschmer, E.; Engelmann, S.; Green, W. M. J.; Weiss, S. M. Experimental realization of deep-subwavelength confinement in dielectric optical resonators. *Science Advances* **2018**, *4*, eaat2355.
(31) Hong, I.; Hong, C.; Tutanov, O. S.; Massick, C.; Castleberry, M.; Zhang, Q.; Jeppesen, D. K.; Higginbotham, J. N.; Franklin, J. L.; Vickers, K.; Coffey, R. J.; Ndukaife, J. C. Anapole-Assisted Low-Power Optical Trapping of Nanoscale Extracellular Vesicles and Particles. *Nano Lett.* **2023**, *23*, 7500−7507.
(32) Möller, F. M.; Holzmeister, P.; Sen, T.; Acuna, G. P.; Tinnefeld, P. Angular modulation of single-molecule fluorescence by gold nanoparticles on DNA origami templates. *Nanophotonics* **2013**, *2*, 167−172.
(33) Kuzyk, A.; Jungmann, R.; Acuna, G. P.; Liu, N. DNA Origami Route for Nanophotonics. *ACS Photonics* **2018**, *5*, 1151−1163.
(34) Humbert, M.; Hallez, Y.; Larrey, V.; Fournel, F.; Palleau, E.; Paillard, V.; Cuche, A.; Ressier, L. Versatile, rapid and robust nanopositioning of single-photon emitters by AFM-nanoxerography. *Nanotechnology* **2022**, *33*, 215301.
(35) Xiong, M.; Sakanas, A.; Dimopoulos, E.; Christiansen, R. E.; Semenova, E.; Sigmund, O.; Yu, Y.; Yvind, K.; Mørk, J. Experimental Realization of Topology-Optimized InP Photonic Cavities with Extreme Dielectric Confinement. *OSA Advanced Photonics Congress 2021* **2021**, No. IM2A.7.
(36) Glembockyte, V.; Grabenhorst, L.; Trofymchuk, K.; Tinnefeld, P. DNA Origami Nanoantennas for Fluorescence Enhancement. *Acc. Chem. Res.* **2021**, *54*, 3338−3348.
(37) Wenger, J.; Rigneault, H. Photonic Methods to Enhance Fluorescence Correlation Spectroscopy and Single Molecule Fluorescence Detection. *IJMS* **2010**, *11*, 206−221.
(38) Wohland, T.; Maiti, S.; Macháň, R. *An Introduction to Fluorescence Correlation Spectroscopy*; IOP Publishing, 2020.
(39) Regmi, R.; Al Balushi, A. A.; Rigneault, H.; Gordon, R.; Wenger, J. Nanoscale volume confinement and fluorescence enhancement with double nanohole aperture. *Sci. Rep* **2015**, *5*, 15852.
(40) Flauraud, V.; Regmi, R.; Winkler, P. M.; Alexander, D. T. L.; Rigneault, H.; van Hulst, N. F.; García-Parajo, M. F.; Wenger, J.; Brugger, J. In-Plane Plasmonic Antenna Arrays with Surface Nanogaps for Giant Fluorescence Enhancement. *Nano Lett.* **2017**, *17*, 1703−1710.
(41) Punj, D.; Mivelle, M.; Moparthi, S. B.; van Zanten, T. S.; Rigneault, H.; van Hulst, N. F.; García-Parajó, M. F.; Wenger, J. A plasmonic 'antenna-in-box' platform for enhanced single-molecule analysis at micromolar concentrations. *Nat. Nanotechnol.* **2013**, *8*, 512−516.
(42) Puchkova, A.; Vietz, C.; Pibiri, E.; Wünsch, B.; Sanz Paz, M.; Acuna, G. P.; Tinnefeld, P. DNA Origami Nanoantennas with over 5000-fold Fluorescence Enhancement and Single-Molecule Detection at 25 M. *Nano Lett.* **2015**, *15*, 8354−8359.
(43) Chengfeng, P.; Shutao, Z.; Farsari, M.; Oh, S. H.; Yang, J. K. W. Nanofabrication: the unsung hero in enabling advances in nanophotonics. *Nanophotonics* **2023**, *12*, 1359−1361.
(44) Lyon, D.; Hubler, A. Gap size dependence of the dielectric strength in nano vacuum gaps. *IEEE Trans. Dielectr. Electr. Insul.* **2013**, *20*, 1467−1471.
(45) Manfrinato, V. R.; Zhang, L.; Su, D.; Duan, H.; Hobbs, R. G.; Stach, E. A.; Berggren, K. K. Resolution Limits of Electron-Beam Lithography toward the Atomic Scale. *Nano Lett.* **2013**, *13*, 1555−1558.
(46) Enderlein, J.; Gregor, I. Using fluorescence lifetime for discriminating detector afterpulsing in fluorescence-correlation spectroscopy. *Rev. Sci. Instrum.* **2005**, *76*, 033102.
(47) Ansys Lumerical FDTD *3D Electromagnetic Simulator*, release R1.3, 2021. https://www.ansys.com/products/photonics/fdtd (accessed 2023-05-03).

https://doi.org/10.1021/acs.nanolett.3c03773
Nano Lett. 2024, 24, 2437−2443